Journal of Ceramic Processing Research. Vol. 22, No. 5, pp. 584~589 (2021)
(Received 7 May 2021, Received in revised form 5 July 2021, Accepted 17 July 2021)
https://doi.org/10.36410/jcpr.2021.22.5.584

J O U R N A L O F
Ceramic Processing Research

Effect of TiO_2 photoelectrode thickness on the performance of dye-sensitized solar cells

Woon-Yong Park[a] and Ki-Tae Lee[a,b,c,*]
[a]*Division of Advanced Materials Engineering, Jeonbuk National University, Jeonbuk 54896, Republic of Korea*
[b]*Department of Energy Storage/Conversion Engineering of Graduate School, Jeonbuk National University, Jeonbuk 54896, Republic of Korea*
[c]*Hydrogen and Fuel Cell Research Center, Jeonbuk National University, Jeonbuk 54896, Republic of Korea*

TiO_2 photoelectrodes for dye-sensitized solar cells (DSSCs) were fabricated by changing the thickness using screen printing method. The amount of dye adsorbed on TiO_2 increases as the thickness of the TiO_2 photoelectrode increases because of the increase in the dye molecule adsorption site. The performance of DSSCs increases up to a TiO_2 thickness of approximately 12 μm, indicating a tendency of dye adsorption that enables photocurrent generation. However, when TiO_2 is thicker than 12 μm, the TiO_2 films start to break, resulting in a decrease in the performance. The optimum thickness of the TiO_2 photoelectrode was 12 μm, which has a low charge transfer resistance.

Keywords: dye-sensitized solar cells, photoelectrode, TiO_2, screen printing, dye adsorption

Introduction

Dye-sensitized solar cells (DSSCs) are one of the most attractive solar cells because of their low manufacturing cost, high conversion efficiency, and wide application compared with conventional silicon-based solar cells [1-4]. A conventional DSSC is composed of a photoelectrode, counter electrode, dye, and electrolyte [5]. The TiO_2 photoelectrode specifically generates photocurrent by absorbing the light, which is one of the most important factors of DSSCs. The material of the photoelectrode is an n-type semiconductor oxide with a wide energy band gap of 3–4 eV, such as TiO_2, ZnO, and SnO_2 [6-10]. TiO_2 is the most widely used ceramic material for photoelectrodes because of its large surface area in adsorbing dye molecules, suitable band edge levels for charge injection/extraction, and high chemical stability [11-16]. Various factors affect the open-circuit voltage (V_{OC}), short-circuit current density (J_{SC}), and fill factor (FF), which are parameters that determine the photoelectric conversion efficiency. In particular, the thickness of the TiO_2 photoelectrode is related to the transfer of electrons, diffusion, and generation of current, which are key factor that influence the overall performance of DSSCs [17-21, 22]. Therefore, the ceramic processing control to fabricate photoelectrode thin films is one of major issues to improve the performance of DSSCs.

In this study, TiO_2 photoelectrodes with various thicknesses were fabricated by a screen printing method. Commercial TiO_2 paste was also used because the efficiency and characteristics of the photoelectrode can be changed depending on the type of TiO_2 paste. The electrical properties and efficiency of the cells were measured, and the electrochemical process inside the DSSC was analyzed. Finally, the change in DSSC mechanism with the thickness of TiO_2 was confirmed using electrochemical analysis.

Experimental Procedure

Fabrication of TiO_2 photoelectrode

Fluorine-doped tin oxide (FTO)-coated glass (TEC 8, Pilkington, UK) with a sheet resistance of 6–9 Ω/□ was sequentially cleaned in acetone (99.5%, Daejung Chemicals and Metals Co., Korea), 2-propanol (99+%, Alfa Aesar, USA) and deionized (DI) water for 10 min each and dried using an air gun. A screen printing method was used with TiO_2 paste (Ti-Nanoixde T/SP, Solaronix, Swiss) for mesoporous TiO_2 film deposition. First, TiO_2 paste was deposited using a screen printer. The screen-printed samples were dried at room temperature for 20 min and then dried again at 120 ºC for 40 min in a dry oven to remove the organic solvent. As shown in Fig. 1(a), a series of steps constitutes one cycle, and the thickness is adjusted as the cycle repeats (1-6 cycles). After finishing the TiO_2 paste deposition, the films were sintered at 500 ºC for 30 min in an ambient atmosphere box furnace and the heating rate

*Corresponding author:
Tel : +82-63-270-2290
Fax: +82-63-270-2386
E-mail: ktlee71@jbnu.ac.kr

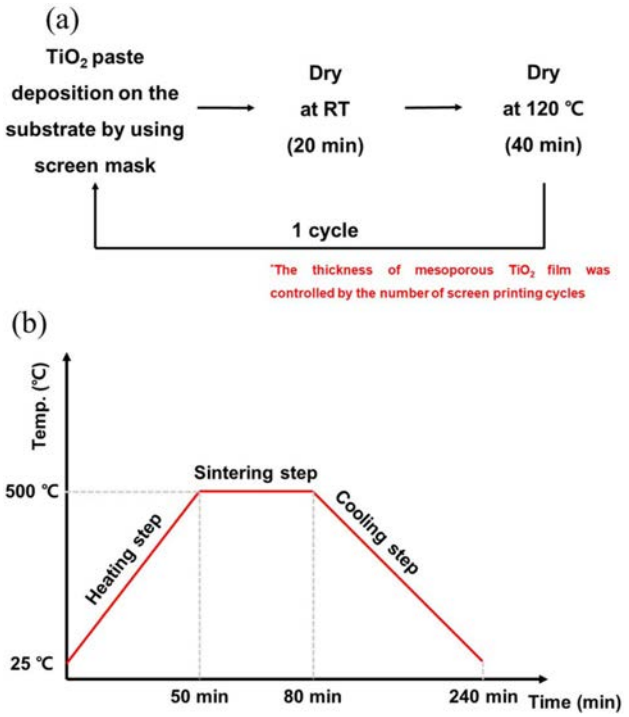

Fig. 1. (a) Schematic of the TiO_2 film deposition cycles for screen printing and (b) the chamber temperature profile corresponding to time.

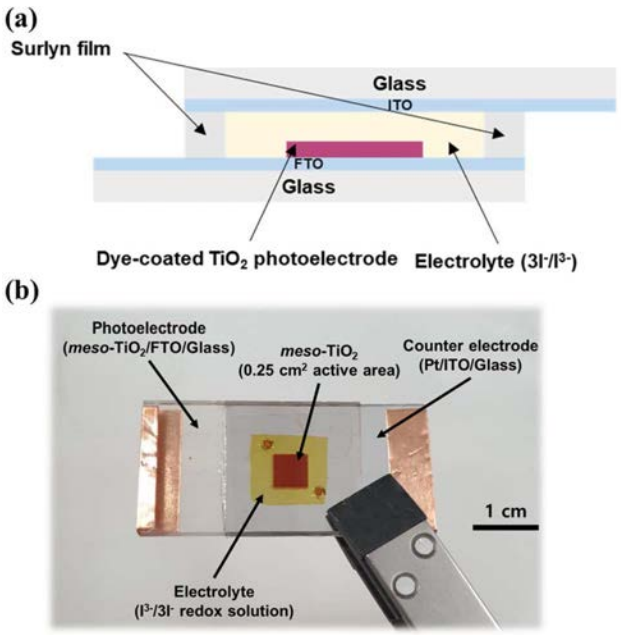

Fig. 2. (a) Schematic diagram of the structure of dye-sensitized solar cells and (b) photograph of the DSSC.

was 10 ºC/min (Fig. 1(b)). The final thickness of the TiO_2 film was controlled according to the number of screen printing cycles.

Assembly of DSSCs

After finishing the sintering step, the TiO_2 films were dipped with the prepared 0.3 mM (bis(tetrabutylammonium)-cis-di(thiocyanato)-N,N'–bis(4-carboxylato-4'-carboxylic acid-2,2-bipyridine) ruthenium (II) ethanol-based solution (N719, Solaronix, Swiss) in a dark field at room temperature for 24 h. Before fabricating the counter electrode, two holes to inject the electrolyte were created in an indium-doped tin oxide (ITO)-coated glass (STN 10, UID, Korea) with a sheet resistance of 6-9 Ω/□, and then washed in the same process as for FTO/glass. Pt film as a counter electrode was deposited on the prepared ITO/glass using DC sputtering equipment (E-1030, Hitachi, Japan) at 25 mA and 30 s (the thickness of Pt: ~5 nm). For assembling the DSSC cells, the prepared photoelectrode and counter electrode were sealed using a 60 μm surlyn film (Solaronix, Switzerland). Electrolyte with the iodide/triiodide (I^-/I^{3-}) redox couple in acetonitrile solvent (AN-50, Solaronix) was injected through the holes. After finishing the electrolyte injection, the holes were enclosed by a cover glass or polyimide tape. The active area of TiO_2 photoelectrode and electrolyte injection was 0.25 cm^2 and 1.2 cm^2, respectively. The final DSSC cells were denoted as TSP×1, TSP×2, TSP×3, TSP×4, TSP×5, and TSP×6 according to the number of screen printing cycles. The schematic diagram of the structure and a photograph of the DSSC cells are shown in Fig. 2.

Characterization

The thickness of the TiO_2 films were analyzed by a high-resolution scanning electron microscope (HR-SEM, SU8230, Hitachi, Japan). Current-voltage (I–V) characteristics of the DSSCs were obtained under a standard illumination condition (100 mW/cm^2 AM 1.5G) using source meter (Keithely 2400, Tektronix, Inc. USA) in the range of ±1 V, at a scan step of 0.02 V and during a delay time of 0.50 s. Electrochemical impedance spectroscopy (EIS) analysis was evaluated with a frequency range of 9 mHz to 100 kHz in a similar standard illumination condition using a potentiostat (SP150, Biologic SAS, France) to confirm the change in the electrochemical component in the DSSCs. The results of the I–V curve and EIS were analyzed with the averages values of at least six individual cells. Electrochemical parameters were obtained from the equivalent circuit and AC impedance spectra using the Zsim mode in the EC-Lab® analysis software.

Results and Discussion

In the case of the screen printing process, the thickness of the film can be changed depending on the organic binder, particle size of the deposition materials constituting the paste, and the distance between the screen mask and substrate. The thickness of the TiO_2 mesoporous film according to the number of screen printing cycles observed by HR-SEM is shown in Fig. 3(a). The thickness of the TiO_2 films increased as the number of

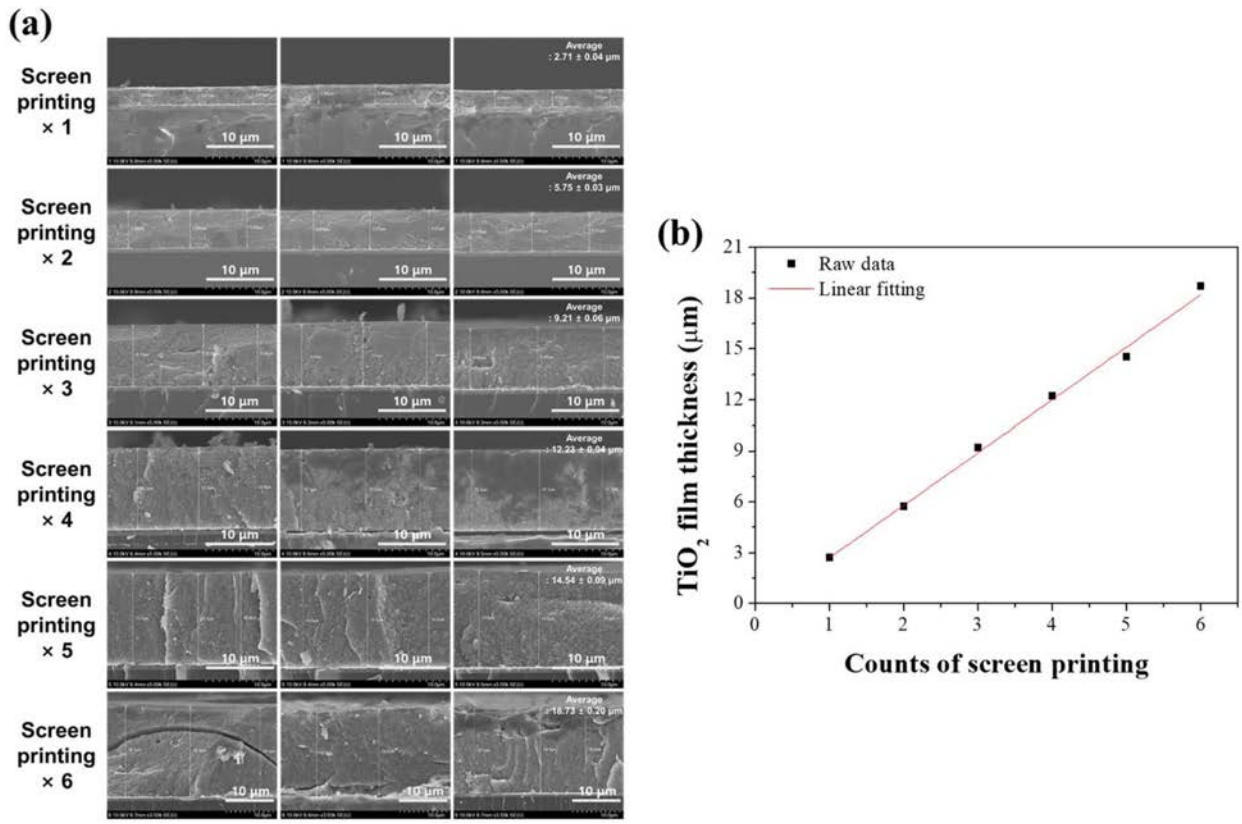

Fig. 3. (a) HR-SEM images and (b) thickness change of the TiO_2 film deposited by 1–6 cycles of screen printing.

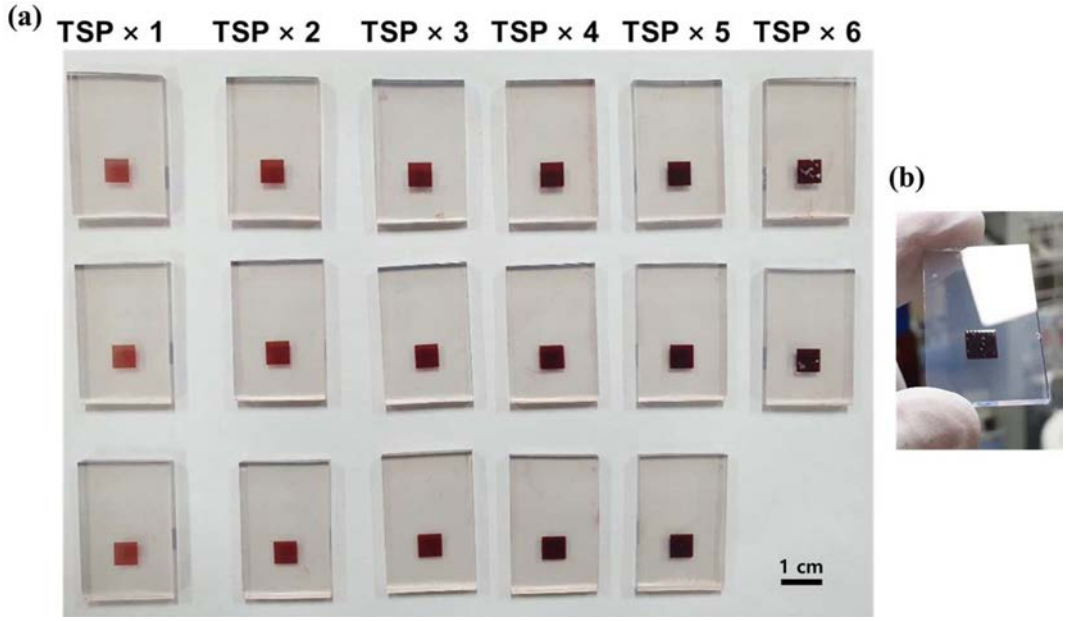

Fig. 4. Images of the (a) TiO_2 film color change according to cycles of screen printing after dye loading process and (b) TSP×5 film to show a crack on the TiO_2 surface.

printings increased. Fig. 3(b) also shows the variation of thickness of the TiO_2 films with screen printing. The thickness increases linearly by approximately 3 μm with each cycle.

As shown in Fig. 4(a), the color of the film after the dye loading process became darker as the thickness of the TiO_2 film increased. However, after five times screen printing (an approximately 12-μm thick film), a surface crack on the TiO_2 film was observed. In the sample with 6 cycles of screen printing, parts of the TiO_2 films were broken, as shown in Fig. 4(b).

UV-visible spectroscopy analysis was performed to

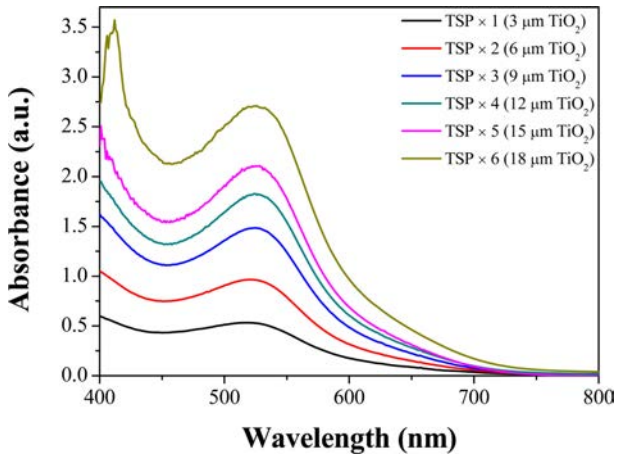

Fig. 5. UV-visible spectroscopy of N719-absorbed TiO_2/FTO/Glass according to the changes in TiO_2 photoelectrode thickness (Blank: TiO_2 film/FTO/Glass).

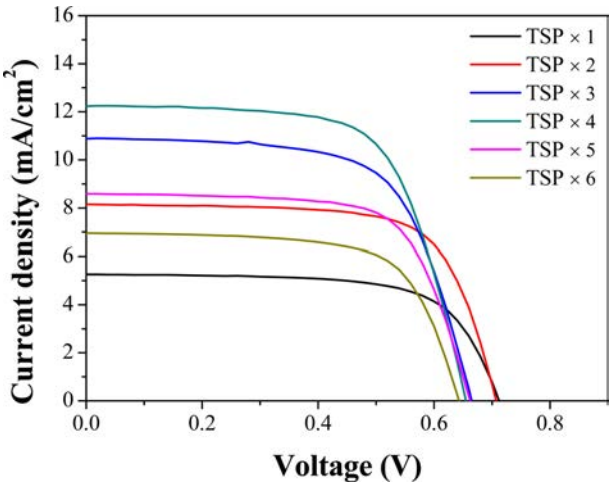

Fig. 6. Photocurrent density-voltage curves of DSSCs with the TiO_2 film thickness change.

confirm the change in the adsorption amount of the N719 dye according to the change in the thickness of the TiO_2 photoelectrode (Fig. 5). Similar to the color change tendency in Fig. 4, the absorbance in the 525-535 nm wavelength range had a tendency to increase as the thickness of the TiO_2 photoelectrode increased [23, 24]. Therefore, the amount of dye adsorption increased by increasing the TiO_2 mesoporous film thickness.

I–V characteristic measurements were performed to confirm the performance according to the change in the thickness of mesoporous TiO_2 films and the parameters are listed in Table 1. As shown in Fig. 6, the efficiency increases as the thickness increases for up to 4 screen printing cycles. Noticeably, the current density increases with increasing thickness corresponding to the tendency of efficiency. The increase in the concentration of electron generation is because of the increase in the adsorption amount of the dye as the TiO_2 thickness increases, resulting in an increase in Fermi level in the TiO_2 conduction band, following an increase in current density with up to four screen printing cycles (12-μm thick). However, after four cycles printing, the performance of DSSC tended to decrease. According to the previous studies, the DSSC performance decreased when the photoelectrode had a critical thickness because of the reduced light transmittance and increased recombination, leading to a reduction in the electron generation and current density [25,26]. However, in this study, surface cracks were observed in the samples with a thickness of 15 μm (five screen printing cycles) and 18 μm (6 screen printing cycles), as shown in Fig. 3 and Fig. 4(b). The decrease in current density and performance after the fourth screen printing cycle is attributed to the surface crack generated when the deposition is too thick. The V_{OC} has a tendency to decrease gradually as the thickness increased because the TiO_2 photoelectrode creates a surface trap level on the TiO_2 surface, resulting in an increase in the recombination with the electrolyte and consequent reduction in the V_{OC} [22, 27]. Moreover, our results demonstrate that the obtained performances are comparable with several literatures [28-31] (Table 1).

EIS was performed to confirm the electrochemical change in the DSSC according to the thickness change

Table 1 Short-circuit current (I_{SC}), open-circuit voltage (V_{OC}), maximum power, fill factor (FF), and power-conversion efficiency (η) of the DSSCs according to the TiO_2 film thickness change.

Sample	V_{OC} [V]	I_{SC} [mA/cm^2]	P_{Max} [mW]	FF [%]	Efficiency [%]
TSP × 1	0.704±0.002	5.733±0.434	0.688±0.050	68.39±0.09	2.753±0.199
TSP × 2	0.696±0.003	8.356±0.321	1.026±0.041	70.49±0.14	4.103±0.164
TSP × 3	0.671±0.006	10.342±0.685	1.147 ±0.058	66.84±0.88	4.588±0.232
TSP × 4	0.665±0.004	11.267±0.948	1.258 ±0.093	66.66±0.83	5.031±0.373
TSP × 5	0.656±0.006	8.155±0.150	0.927 ±0.020	69.30±0.35	3.708±0.081
TSP × 6	0.641±0.004	6.716±0.304	0.732 ±0.028	68.07±0.43	2.928±0.114
Hydrothemal TiO_2 [28]	0.7111	11.34	-	66.57	5.7
Flame spray pyrolysis TiO_2 [29]	0.72	5.25	2.44	64	2.44
O_2 plasma treatment of TiO_2 [30]	0.80	7.59	-	66	4.0
Aerosol deposition TiO_2 [31]	0.72	8.08	-	69.41	4.07

*The analysis results of I-V curve are the averages of at least 6 individual cells.

Table 2 Electrochemical resistance and capacitance of illuminated DSSCs of the TiO_2 photoelectrode according to TiO_2 film thickness change under open circuit conditions. Data were obtained from EIS fits using the equivalent circuits in Fig. 7.

Sample	R_S [Ω]	R_{ct1} [Ω]	C_{CE} [mF]	R_{ct2} [Ω]	C_μ [mF]	R_W [Ω]	t_W [s]
TSP × 1	23.720±1.271	1.944±0.067	0.023±0.006	16.833±1.154	0.131±0.012	2.682±0.678	1.274±0.432
TSP × 2	17.267±0.674	2.619±0.280	0.036±0.008	8.770±0.066	0.215±0.010	3.634±0.255	2.788±0.561
TSP × 3	21.305±1.606	2.683±0.740	0.138±0.093	5.204±0.945	0.233±0.114	2.994±0.346	2.321±0.683
TSP × 4	17.535±0.325	4.609±0.556	0.049±0.001	4.612±0.501	0.349±0.000	3.186±0.234	2.205±0.229
TSP × 5	19.377±0.483	3.534±0.154	0.011±0.001	6.513±0.233	0.294±0.005	4.526±0.248	2.139±0.167
TSP × 6	18.868±0.076	3.444±0.134	0.012±0.0003	7.088±0.395	0.254±0.053	4.524±0.320	1.819±0.242

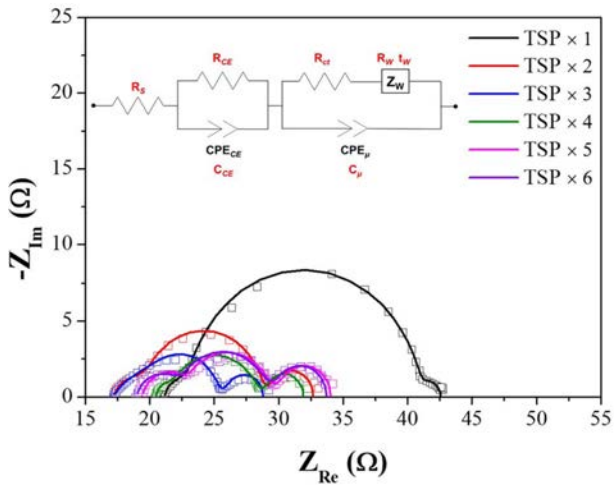

Fig. 7. AC impedance spectra of DSSCs according to the TiO_2 film thickness change (Dot: Raw data, Line: fitting data from equivalent circuit).

of the TiO_2 films. Fig. 7 shows the Nyquist plots of the electrochemical impedance spectra of the DSSC for changing the thickness of the TiO_2 photoelectrode. In a conventional DSSC, the three semicircles are drawn on the Nyquist plot in EIS data, which is designated to a redox reaction of $3I^-/I^{3-}$ at the Pt counter electrode (the first semicircle in the high frequency range), charge transfer reaction at the interface between TiO_2/N719 and electrolyte (the second semicircle in the middle frequency range), and the Warburg diffusion process of iodide (the third semicircle in the low frequency range) [27, 32]. The electrochemical parameters obtained by the simulation of fitting between equivalent circuit and impedance spectra are listed in Table 2. The measured impedance data (dots) are well matched with the modeling data (lines) calculated by the equivalent circuit and electrochemical parameters. As shown in Fig. 7 and Table 2, the resistance of the charge transfer reaction in the TiO_2/dye-electrolyte interface decreased as the thickness of TiO_2 increased up to a thickness of 12 μm, and increased at thicker TiO_2. This result is consistent with the tendency of the current density and efficiency in I–V characteristics. Alternative to the tendency of the charge transfer resistance, the capacitance of the charge transfer increases up to a thickness of 12 μm and then decreases at thicker TiO_2. The tendency of impedance parameters in changing the thickness of the TiO_2 is in agreement with previous studies in that one of the factors that increases the performance as the thickness increases is an increase in current density because of a decrease in charge transfer resistance, and the increase in charge transfer capacitance is related to the total density of electrons [32-34].

Conclusions

TiO_2 mesoporous films were fabricated using a screen printing method with thickness of 3 μm/screen prints as determined by FE-SEM. As the thickness of TiO_2 films increased to 12 μm, the performance of the DSSCs increased. I–V measurements showed the highest efficiency in the 12-μm thick film. The increase in overall performance may be because of the increase in current density (ISC: 11.267 mA/cm^2 in the 12 μm TiO_2 films). However, the efficiency tends to decrease with TiO_2 thicker than 12 μm. The EIS demonstrated that the resistance of the TiO_2/dye-electrolyte charge transfer reaction corresponding to the second semicircle in the Nyquist plot decreases up to a thickness of 12 μm and then increases, which is consistent with the tendency in I–V measurements. As the thickness of the TiO_2 film increases, more current was generated because of an increase in the amount of dye loading, resulting in an increase in the performance. As the thickness increases, the amount of dye loading increased; however, the DSSC performance decreased at TiO_2 thicker than 12 μm. This performance decrease was attributed to the connection break among TiO_2 particles by surface cracking caused by stress differences between FTO/TiO_2 and the TiO_2 particle interface.

Acknowledgements

This research was supported by "Research Base Construction Fund Support Program" funded by Jeonbuk National University in 2020. This work was supported by the National Research Foundation of Korea (NRF) grant funded by the Korea government (MSIT) (No. 2018R1A4A1025528). This work was also supported by the Technology Development Program to Solve Climate Changes of the National Research Foundation (NRF) grant funded by the Korea government

(Ministry of Science and ICT) (2017M1A2A2044930).

References

1. B. O'Regan and M. Grätzel, Nature 353[6346] (1991) 737-740.
2. P. Ramasamy, M.-S. Kang, H.-J. Cha, J. Kim, Mater. Res. Bull. 48[1] (2013) 79-83.
3. L. Zhao, J. Yu, J. Fan, P. Zhai, S. Wang, Electrochem. Commun. 11[10] (2009) 2052-2055.
4. S.K. Park, C. Chung, D.-H. Kim, C. Kim, S.-J. Lee, Y.S. Han, Mater. Res. Bull. 47[10] (2012) 2722-2725.
5. M. Gratzel. Nature 414[6861] (2001) 338-344.
6. K. Patil, S. Rashidi, H. Wang, W. Wei, Int. J. Photoenergy 2019 (2019) Article ID 1812879.
7. J.H. Kim, K.J. Lee, J.H. Roh, S.W. Song, J.H. Park, I.H. Yer, B.M. Moon, Nano. Res. Lett. 7 (2012)1-12.
8. M.U. Rahman, M. Wei, F. Xie, M. Khan, Catalysts 9[3] (2019) 273.
9. R. Kasaudhan, H. Elbohy, S. Sigdel, H. Qiao, Q. Wei, Q. Qiao, IEEE Electron Device Lett. 35[5] (2014) 578-580.
10. P. Sanjay, I. Isaivani, K. Deepa, J. Madhavan, S. Senthil, Mater. Lett. 244 (2019) 142-146.
11. R. Vittal, K.-C. Ho, Renewable Sustainable Energy Rev. 70 (2017) 920-935.
12. N.I. Beedri, P.K. Baviskar, V.P. Bhalekar, C.V. Jagtap, Inamuddin, A.M. Asiri, S.R. Jadkar, H.M. Pathan, Phys. Status Solidi A 215[18] (201) 1800236.
13. J.-J. Lee, M.M. Rahman, S. Sarker, N.C.D. Nath, A.J.S. Ahammad, J.K. Lee, Adv. Compos. Mater. Med. Nanotechnol. 182 (2011) 210-218.
14. S.N.F. Zainudin, H. Abdullah, M. Markom, J. Mater. Sci. 30[6] (2019) 5342-5356.
15. B. Roose, S. Pathak, U. Steiner, Chem. Soc. Rev. 44[22] (2015) 8326-8349.
16. C.C. Raj, R. Prasanth, J. Power Sources 317 (2016) 120-132.
17. H.-W. Lin, Y.-S. Wang, Z.-Y. Huang, Y.-M. Lin, C.-W. Chen, S.-H. Yang, K.-L. Wu, Y. Chi, S.-H. Liu, P.-T. Chou, Phys. Chem. Chem. Phys. 14[41] (2012) 14190-14195.
18. J.A. Anta, F. Casanueva, G. Oskam, J. Phys. Chem. B 110[11] (2006) 5372-5378.
19. K.-M. Lee, V. Suryanarayanan, K.-C. Ho, Sol. Energy Mater. Sol. Cells 90[15] (2006) 2398-2404.
20. K. Zhu, N. Kopidakis, N.R. Neale, J. van de Lagemaat, A.J. Frank, J. Phys. Chem. B 110[50] (2006) 25174-25180.
21. K. Zhu, S.-R. Jang, A.J. Frank, J. Phys. Chem. Lett. 2[9] (2011) 1070-1076.
22. S.R. Raga, E.M. Barea, F. Fabregat-Santiago, J. Phys. Chem. Lett. 3[12] (2012) 1629-1634.
23. P. Wen, Y. Han, W. Zhao, Int. J. Photoenergy 2012 (2012) Article ID 906198.
24. F. De Angelis, S. Fantacci, E. Mosconi, M.K. Nazeeruddin, M. Grätzel, J. Phys. Chem. C 115[17] (2011) 8825-8831.
25. V. Baglio, M. Girolamo, V. Antonucci, A.S. Aricò, Int. J. Electrochem. Sci 6[8] (2011) 3375-3384.
26. M.G. Kang, K.S. Ryu, S.H. Chang, N.G. Park, J.S. Hong, K.-J. Kim, Bull. Korean Chem. Soc. 25[5] (2004) 742-744.
27. S. Nakade, M. Matsuda, S. Kambe, Y. Saito, T. Kitamura, T. Sakata, Y. Wada, H. Mori, S. Yanagida, J. Phys. Chem. B 106[39] (2002) 10004-10010.
28. S.N. Karthick, K.V. Hemalatha, C.J. Raj, H.-J. Kim, M. Yi, J. Ceram. Proc. Res. 13[S1] (2012) 136-139.
29. A. Aboulouard, B. Gultekin, M. Can, M. Erol, A. Jouaiti, B. Elhadadi, C. Zafer, S. Demic, J. Mat. Res. Tech. 9[2] (2020) 1569-1577.
30. Y. Kim, B.J. Yoo, R. Vittal, Y. Lee, N.-G. Park, K.-J. Kim, J. Power Sources 175[2] (2008) 914-919.
31. D. Kim, K. Lee, H. Lee, J. Lim, J. Park, J. Kor. Cryst. Growth and Cryst. Tech. 30[2] (2020) 61-65.
32. J. Bisquert, M. Grätzel, Q. Wang, F. Fabregat-Santiago, J. Phys. Chem. B 110[23] (2006) 11284-11290.
33. J. Bisquert, J. Phys. Chem. B 106[2] (2002) 325-333.
34. F. Fabregat-Santiago, J. Bisquert, E. Palomares, L. Otero, D. Kuang, S.M. Zakeeruddin, M. Grätzel, J. Physic. Chem. C 111[17] (2007) 6550-6560.